DEPARTMENT OF THE INTERIOR

U. S. GEOLOGICAL SURVEY

MONTE CARLO SIMULATION OF PEAK-ACCELERATION ATTENUATION USING A FINITE-FAULT UNIFORM-PATCH MODEL: A PARAMETER STUDY

BY A. M. ROGERS AND D. M. PERKINS[1]

Open-File Report 95-5

[1]U.S. Geological Survey, Box 25046, MS 966, Denver, Colorado 80225

1995

Contents

Illustrations

Tables

Introduction

Prediction of peak acceleration for engineering uses continues to be of interest, particularly for the design of ordinary structures, for the purpose of producing probabilistic hazard maps, and for assessing the ground-failure hazard (liquefaction, slumping) induced by earthquake shaking. The most common procedures for predicting peak accelerations are based on equations derived from regression analysis of large data sets or from stochastic modeling. Although both of these techniques produce results of practical merit and wide application, assumptions that underlie both methods may result in biased predictions. Regression results, for example, can be biased by the choice of functional form. Different functional forms produce different predictions, particularly in the very near and very far field, where the functional forms extrapolate into areas not well controlled by data. Stochastic modeling of peak acceleration is commonly based on point-rupture models, so that properties, which ought to depend on the finite extent of the source, are not represented for these models.

Other more rigorous methods have been used in the prediction of peak accelerations. In some of these studies, finite-fault models were subdivided into patches and the ground motion was synthesized by summing Green's functions contributions from each patch (i.e., Joyner, Campbell, and Harmsen, 1988; Saikia, 1994; Silva, Roblee, and Abrahamson, 1995; Somerville, Sen, and Cohee, 1991). Our approach is similar to these studies with additional simplifications as noted below. The fundamentally different aspect of this study is that we demonstrate that peak acceleration scaling with magnitude can be produced by the characteristics of extreme values and does not depend on the random addition of high-frequency energy alone.

The goal of this study was to evaluate the magnitude- and distance-dependent peak-acceleration scaling using a physical model of the earthquake source. In an earlier study (Perkins, Rogers, and Campbell, in prep.), using a data set without magnitude or distance preselection, we observed smoothed peak accelerations that increased with magnitude in a manner that was distance dependent and also featured near-field reduction in the magnitude dependence with increasing magnitude. In the present study, we evaluate a fault ground-motion model that has the potential to fit these smoothed data across broad distance and magnitude ranges. This model includes statistical effects likely to affect the peak-acceleration mean in a large data set. The use of a finite fault with statistical properties permitted us to determine the form of peak-acceleration attenuation curves without a priori assumptions about their shape or scaling properties, such as commonly required in fitting parametric functional forms with regression analysis.

Definitions and Conventions

First, we define terms used in the discussion. Magnitude scaling (or simply scaling) of peak acceleration refers to the increase in peak acceleration with increasing magnitude at a given distance (da_p/dM). Peak-acceleration curves may have constant magnitude scaling ($da_p/dM = \text{constant}$), such that the increase in peak acceleration for a unit increase in magnitude is independent of magnitude. For many regression studies, $da_p/dM = \text{constant}$ is assumed for all distances. Magnitude saturation refers to the case when $da_p/dM < 0$. This effect could be constant at all distances, or it too could be a function of distance. We refer to the latter case as distance-dependent magnitude saturation.

Given a real peak acceleration sample, triggering bias is an increase of the mean peak acceleration at a given distance and magnitude produced by the fact that lower acceleration values for earthquakes having the same magnitude and distance are not recorded below some preset instrument threshold (McLaughlin, 1991). Hence, at some distances only the upper part of the peak-acceleration distribution may be observed. This effect biases the mean peak acceleration at these distances to larger values in a manner that is dependent on both distance and magnitude. As described below, we simulate this effect in our statistical model.

Most of our model results and actual data are plotted in terms of the variable "*Z*", which is the mean (for 100 realizations) of the $log(a_p)$ with a first-order geometric correction applied

(*0.853log(closest distance to the fault)* is added to the a_p). *Z* is plotted at the closest distance to the fault because the data with which we wish to compare is plotted in this manner. The size of this correction is arbitrary, but the value chosen represents the first-order attenuation observed in the data set. This transformation, produces curves in which differences in scaling show more clearly than when simply plotting $log(a_p)$ vs. $log(R)$ for which increases in geometric or anelastic attenuation produce curves apparently closer together even if magnitude scaling is constant.

A Smoothed Peak-Acceleration Data Set

Our data are from 180 earthquakes with magnitudes ranging from about 3 to 8 and 1241 recordings world wide at source-station distances ranging from a few kilometers to about 400 km (Campbell, written communication, 1990). These data have not been preselected on any basis. Our purpose in fitting unpreselected data sets is that preselection of data to minimize fitting difficulties, such as sampling bias, significantly reduces the data available in a data set that is already sparse. Furthermore, data selection reduces the capacity to distinguish the effect of fitting alternative function forms. That is, either of two functional forms may fit the selected data equally well, even though predictions into non-data portions of *M-log R* space may be very different.

In a previous paper (Perkins, Rogers, and Campbell, in prep.) we adopted an objective smoothing procedure to reduce the dispersion in the data. The data were smoothed in several stages that can essentially be described as follows. First, the peak acceleration values were binned in narrow distance ranges to eliminate distance dependence. Next, a non-parametric least-squares smoothing technique (locally-weighted least squares, (i.e., McLain, 1974)) was applied to the data in a given bin with magnitude as the independent variable. This process produces smoothed peak acceleration curves for each bin as a function of magnitude. We interpolate these curves to obtain values at unit magnitudes and plot these values at the midpoint of the bin. Finally, the interpolated values are connected for a given magnitude unit to form smoothed peak acceleration attenuation curves as a function of distance with magnitude as a parameter, as shown in figure 1a.. This representation of the data is perhaps the most complete view of the characteristics of peak-acceleration attenuation yet presented because it is based on a very large data set that has not been preselected with respect to magnitude or distance ranges. Our smoothed peak-acceleration curves demonstrate: (1) magnitude scaling; (2) magnitude saturation for distance slices less than about 30 km; (3) magnitude- and distance-dependent bias produced by instrument triggering thresholds; (4) an increase in scaling for M6-8 for distance slices beyond 30 km; and (5) a convergence of all the curves beyond 80 km.

Note that these data have not been smoothed in a way that would remove the triggering bias. The data as presented include triggering bias. When fitting the model to these data, we include a term that produces bias in the model results. Our plan in this case would be to obtain a fit to the data with a biased model, but to remove the bias term when predicting unbiased accelerations.

Perkins and others. (in prep.) attempted a subjective alternate fit to the data which was intended to compensate triggering bias. This data fit was termed the paradigm fit because it utilized a magnitude scaling "shape" adopted from the characteristics of the data itself in the close-in distance slices (figure 1c). This shape was assumed to be representative of peak accelerations unaffected by sampling bias at all distances and was fit to each distance-slice data set. Attenuation curves (figure 1b) were then obtained from these fitted curves at unit magnitude intervals as described above. (Note that the paradigm shape assumed variable magnitude saturation in all distance slices). When fitting the model in the present study to the paradigm data, the model bias is arbitrarily set 3 to 4 times lower than the bias determined to fit the original data. The purpose in attempting a fit to the paradigm data set is to determine whether this interpretation reasonably represents something physical or is a simplistic over interpretation. Ideally the same model parameters (except for bias) would produce a good fit to both data sets.

A Geometric-Stochastic Fault Model and Extremal Peak-Acceleration Characteristics

In this study, we evaluate peak-acceleration magnitude and distance scaling using a statistical finite-fault earthquake source model. We term the peak-acceleration characteristics in this model extremal scaling because the peak-acceleration dependence on distance and magnitude is strongly influenced by extreme value statistics, as explained below. We explore the model in two steps. First, we vary the parameters to understand their effects. Second, in a trial and error procedure, we vary the model parameters to fit the smoothed data.

This model is not intended to be a complete representation of the earthquake source. Our intent is only to explore the model's statistical effects without including other source effects, such as isochrone pulse addition. (An isochrone is a locus on a fault with propagating rupture, such that the radiated energy from all points along the locus arrives at a given station at the same time (Bernard and Madariaga, 1984; i.e., Spudich and Frazer, 1984). Preliminary model studies with combined isochrone-extremal effects, however, suggest that the model parameters required to fit the data suppress isochrone-produced scaling relative to extremal-produced scaling. In this case, short pulse durations are the reason for the weak isochrone-produced scaling (Rogers and Perkins, 1994). The isochrone model results will be described in a future paper.

Figure 2 shows the geometric aspects of the two-dimensional fault model. The fault rupture consists of n rectangular patches, each producing one peak-acceleration value drawn from a log-normal random distribution with constant mean and standard deviation. This acceleration is attenuated to a randomly chosen station location on the locus of constant closest distance to the fault (e.g., Campbell, 1985). Both anelastic (e^{-kr}) and geometric ($1/r$) attenuation are applied, where r is the distance between the patch and the station (r_p in figure 1). The fault has random dip, as explained below. Note that, for dipping faults, the locus of constant closest distance is a more complicated figure than that shown. Patch properties are chosen to be magnitude independent in order to accommodate near-field magnitude saturation observed in peak accelerations for magnitudes greater than 6 (Perkins, Rogers, and Campbell, in prep.). The question is whether such a model can also produce scaling in the far field. This paper confirms that such scaling is, in fact, possible. The patches can be viewed as zones of randomly variable stress drop, slip velocity, rupture velocity, or fault strength as has been assumed in a number of past studies, (Andrews, 1980; Andrews, 1981; Boatwright, 1982; Boatwright and Quin, 1986; Frankel, 1991; Spudich and Cranswick, 1984; Spudich and Frazer, 1984). The assumption that each patch radiates one peak value is related to earlier work suggesting that most of the high-frequency energy is released from a compact zone near the rupture front (Heaton, 1990; Madariaga, 1977). Because we are attempting to explain a peak acceleration data set rather than the data from a single earthquake, we assume that radiation pattern effects can be ignored. We further assume that variations in slip velocity or slip direction on the fault plane and or changes in rupture velocity are statistically simulated by the randomization of peak patch accelerations. As we are only interested in the scaling properties of peak acceleration, we consider the peak-acceleration distribution mean to be an artificial construct representing a peak particle acceleration at 1 km from the patch. These assumptions also allow us to set the free surface and component partition effects to unity. Because of our simplfying assumptions, we draw no conclusions about the actual particle-motion properties at the patch from the model parameters required to fit the data. Although the assumptions of this model are somewhat limiting, we suggest that it is more realistic than a point-source stochastic model or that implied by regression models based on distance and magnitude alone.

At a particular site, at a given distance from the fault rupture, each of the patches contributes a peak acceleration that has been attenuated according to the patch-to-site distance. The largest of all the attenuated peak accelerations is adopted as the peak acceleration observed at the site. Neither pulse width, pulse arrival times, nor rupture duration are included in the model. Because we do not model destructive or constructive interference of the pulses, we implicitly assume that no pulses arrive at exactly the same time. This assumption is only approximately valid and may lead to underestimates of the peak values particularly at more distant sites where pulse widths may have

broadened due to anelastic attenuation. Nevertheless, the capacity of this model to replicate data properties suggests that much of the basic physics governing peak-acceleration attenuation can be represented by our simplifying assumptions.

How The Model Produces Peak-Acceleration Scaling

The basic method by which the model produces magnitude scaling of peak acceleration can be explained by reference to extreme statistics theory. Suppose that all the patches are equidistant to some site. In this case, the attenuation would be identical for the contribution of each patch, and the peak acceleration at the site would be the extreme of n identical distributions. Figure 3 demonstrates the characteristics of extremes sampled from an underlying normal distribution. The fundamental characteristics of our model demonstrate asymptotically the properties of a Gumbel Type I distribution, such as that shown in this figure. Several underlying distributions, including the normal distribution, generate extreme values that follow Gumbel Type I statistics (Bury, 1975). Thus, our assumption that the logarithm of peak patch acceleration is drawn from the normal distribution is not critical. As shown in this figure, as the number of samples, n, from the underlying distribution increases, the distribution of the maximum values selected from the sample shifts to a larger value and the distribution of the maxima narrows. Small earthquakes have few patches and large earthquakes have many patches. Thus, we expect that large earthquakes provide the opportunity to sample a larger peak-acceleration extreme. It is this basic premise that produces extremal-related scaling in the model.

The effect is more complicated, however, than this simple illustration shows. First, the effect is distance-dependent because the effective number of patches is controlled by attenuation. The effective number of patches is a subjective term referring to the number of patches that have some practical likelihood of contributing the largest peak acceleration at a given station. For stations near the fault, accelerations arriving from relatively distant patches are attenuated more than those from close patches and, thus, are less likely to be the highest at the station. For stations far from the fault, however, especially those perpendicular to the fault trace ("flank" stations), all patches are at about the same distance from the station. Thus, these distant stations have relatively greater likelihood of sampling farther into the attenuated-acceleration distribution extremes compared to close stations. Stations located off the fault ends ("endcap" stations), however, again "see" primarily the closest patches, and the likelihood of observing increasing ground motions as a function of increasing fault length is again low. Hence, complexity involving distance-dependent and aspect-dependent scaling comes into play. These factors and the narrowing of the extreme distributions as the number of patches increases control peak-acceleration magnitude- and distance-dependent scaling, including magnitude saturation.

The distribution of patch-to-station distance is an indicator of the complexity of the model process. Figure 4 demonstrates the characteristics of the distribution of patch-to-station distances for two values of closest distance to the fault (2.5 and 250 km) and two station azimuths (endcap and flank). The first and second panels show, for instance, that the patch distances for the close station positions vary over a wide range in *log R,* and the distributions are skewed to the distant side of their range. Only the closest patches have significant likelihood of contributing the largest peak acceleration; here, we expect little magnitude dependent scaling. The patch distances for the distant stations, however, have a narrow range in *log R* and tend to be skewed to the close end of their range. In this case, most patches have the opportunity to contribute the largest peak acceleration; here, we expect significant magnitude dependent scaling. These properties lead to complex changes in the number of effective patches as a function of azimuth and distance and, hence, complexity in the extreme sample distributions, as described above.

Other Model Properties

Some subtle features of the station sampling process are also included in the model, although these features do not strongly affect the model results. Our assumption is that the data set we wish to model has stations that are randomly uniformly distributed on the earth's surface around the fault. We require these stations to be located at the same constant-closest distance to the finite fault.

For a vertical fault, this assumption leads to a constant mean station density on any section of the locus of closest distance; whereas, for a dipping fault, the mean station density at downdip locus sections is greater than for updip locus sections. Thus, uniform-area station sampling for a dipping fault leads to variable station density on a locus of constant-closest distance as a function of azimuth from the fault. The details of this sampling process are not significant enough to include here.

The model includes other parameters to simulate effects that we believe are present in the data (Perkins, Rogers, and Campbell, in prep.). For example, we include a detection threshold limit below which a station does not trigger. The detection threshold produces a sampling-bias effect that is simulated in the model by recomputing the station acceleration until a value above the threshold is obtained. The number of times that resampling is permitted before assuming no value at that distance is also a model parameter.

We also include an upper limit on the allowable patch peak acceleration. This limit simulates the strength-of-rock limit on peak acceleration that has been suggested by others (i.e., Brune, 1970). In a later section of this paper, we evaluate the effect of assuming that the patch peak-acceleration mean varies with depth to simulate the effects of varying crustal strength versus depth. For all other sections of this paper, we assume that the distribution mean is a constant and independent of depth. A flow chart describing the basic properties of the calculation procedure is shown in Appendix A.

As noted earlier, destructive or constructive interference of the pulses is not included. The model assumptions implicitly require that either no pulses arrive at exactly the same time or that, if pulses do arrive at the same time, a single patch produces the peak acceleration observed. The contributions along an isochrone are differentially attenuated to a given site because different positions along an isochrone are at different distances from the station. For stations close to the fault, only sections of the isochrone closest to the station may contribute significantly. This fact is a partial justification of our assumptions.

The assumption of minimal interference is also apparently supported by the work of Spudich and Frazer (1984) and Spudich and Cranswick (1984). In figure 11 of Spudich and Fraser, for example, the largest peak acceleration originates from the region between the 1.95 and 2.0 isochrones, which can easily be visualized as a single patch. Figures 21 and 22 in Spudich and Cranswick show a similar result, although the origin of the largest peak on the north-south component in their figure 22 may originate from one or two patches.

Next, we infer the results that might be expected using our basic model modified to accommodate addition of patches along an isochrone. Again, we assume that each patch generates one log-peak value drawn from identical log-normal distributions. In this model, we assume that the largest recorded peak is the sum of n peak values, each of which has been attenuated by its distance to the station. In fact, in this model, all recorded peaks are the sum of one or more attenuated patch values for a succession of isochrones. The largest peak, then, is still a sample drawn from an extreme value distribution because the sum of n log-normal distributions is another log-normal distribution with modified mean and standard deviation. Our simplifying assumptions may be partially justified on this basis.

Parameter Study

In this parameter study, the following are variable: patch size, magnitude, site-to-fault distance, mean and standard deviation of the patch log-peak acceleration, site-threshold peak acceleration, resampling limit, and the patch peak-acceleration maximum. For a given set of parameters, we first fix patch size, select a magnitude from a set of standard integer magnitudes, obtain a fault length from a fault-length vs. magnitude distribution, obtain a fault width, and tile the fault rupture with patches. We then choose one of a given set of standard distances. A station is randomly selected from the locus of sites having that distance as constant closest distance to the rupture. For each patch, a ground motion is obtained from the patch distribution and attenuated to the station. The largest attenuated peak acceleration at the station from all patches is the selected peak acceleration for this trial. If no value above the threshold is obtained, we resample as many as 200 times (nominally, unless stated below). This process is repeated for 100 random station locations. From

these 100 trials (or fewer if resampling produces no values above the threshold), we compute the average of the *log(maximum peak-acceleration values)* of each trial. This process mimics the way in which peak-acceleration data are obtained. The *Z-value* computed from this average is the value that is plotted for the given magnitude and distance. This process is repeated for the remaining standard distances and magnitudes to obtain a suite of *Z-value* curves.

The model parameters are set as follows for the parameter study. For crustal earthquakes, we assume the following values for fault length: *M 4*-1.3 km; *M 5-3.6* km; *M 6-10* km; *M 7-50* km; *M 8-190* km. Fault width equals fault length for *M 4-6*, and the fault mid-point is fixed at 7 km. Hence, all magnitude 4 events, for example, have a depth extent given by $7 \pm width \times \sin(dip)/2$. This assumption leads to ruptures for $M \leq 6$ that are never closer to the surface than 2 km (for 90 degree dip). The fault width for *M 7* is determined both by the dip and depth to the brittle-ductile boundary. We assume this boundary is at 15 km depth for crustal intraplate earthquakes. The dip is assumed to vary randomly between 60 and 90 degrees. For *M 8* earthquakes, we assume a fixed 90 degree dip and 15 km width.

For subduction thrust earthquakes, we assume a fault length of 250 km for *M 8*, a brittle-ductile boundary at 25 km, and fault dip varying randomly between 10 and 20 degrees. Only stations off the downdip fault flanks are used for simulated subduction-zone earthquakes because other potential station locations are assumed to lie offshore. Smaller subduction earthquakes are not considered because we only wish to approximately bound the data. Larger subduction thrust earthquakes are not contained in the data set.

EFFECTS OF THE PATCH PEAK-ACCELERATION DISTRIBUTION

Inasmuch as the patch peak-acceleration distribution is the core of this simulation, we expect that the parameters of this distribution will produce first-order effects. For example, increasing or decreasing the distribution mean should increase or decrease the levels of the *Z-curves,* although not their relative shapes. When upper or lower limits are included, however, the effect of the mean is more complex, as explained below. The effect of the standard deviation (*sigma*) is harder to anticipate, but it should have an effect on the level of the curves because, as standard deviation increases, the upper fractiles controlling the peak ground motions correspond to larger ground motions.

Figure 5 shows the effect of varying the standard deviation for a constant mean *log(peak acceleration)* equal to -0.3 (corresponding to 0.5 g). This figure illustrates how varying the standard deviation affects the relative frequency with which 2.0 g is exceeded. For example, a distribution with standard deviation, *sigma=0.3*, has a probability, *p=0.02*, of generating a value greater than 2 g, but, for a distribution with *sigma=0.6*, *p=0.16*. (The probability of generating a 2 g peak, of course, will also vary if the distribution mean is changed.)

Figure 6 shows a set of *Z-curves* for several values of patch standard deviation with the other parameter values fixed, as shown. As sigma increases, the level of the curves increases as anticipated, and the scaling of peak acceleration with magnitude is more pronounced. Note also that the degree of peak-acceleration saturation with magnitude for a given distance decreases with increasing sigma. The saturation is also distance dependent, that is, saturation is strong at close distances and weak at large distances.

EFFECTS OF PATCH SIZE

Figure 7 illustrates the effects of patch size on the peak-acceleration attenuation. For a given fault size, patch size controls the *number* of effective patches contributing to the sampling of extremes. Decreasing the patch size increases the number of effective patches for any fixed fault size (given magnitude) and, hence, increases the level of the curves. Level change, without large changes in scaling or scaling saturation, is the strongest effect of patch size. As patch size decreases, the separation of the curves for the smallest events first increases and then decreases. This result follows because, for low-magnitude events, small patch sizes (e.g., *patch size=0.5 km*) increase the rate of exceedances for small earthquakes relatively faster than that of the larger

events. Another scaling effect is also observed. At large patch sizes, as the patch size approaches the fault size for small earthquakes (e.g., *patch size=4 km*), small events have the same number of patches and, thus, the same scaling.

EFFECTS OF ACCELEROMETER-TRIGGERING THRESHOLD

For actual strong-motion data sets, as ground-motion levels decline with either declining magnitude or increasing distance, there is a decrease in the likelihood that a strong-motion instrument will trigger. Or, even if triggered, the ground motion may be too low to be considered worthwhile digitizing or reporting. Accordingly, there is a tendency for data to fail to express the full range of ground-motion variability for low magnitudes at a given distance or for large distances at any given magnitude. Thus, at the bottom and right hand edges of real-data *Z-curves*, bias should be present in the data means. The level of ground motion at which this bias is expected could vary, but it is near the instrument triggering level. This level varies among different accelerographs but is commonly in the range 0.01-0.05 g. The lack of values below some level will produce biased overestimates of the mean value beginning at larger distances for larger magnitudes.

Site effects complicate the bias modeling because rock sites may trigger less frequently than soil sites, and hence data near the bias regions are likely to be over represented by soil sites. Inasmuch as soil-site amplification is itself distance dependent (Rogers, Perkins, and others, 1991), the use of a simple site ground-motion threshold to model this bias is not entirely correct.

Our model results (Figure 8a-c) show the sampling bias effect for different triggering thresholds. As the triggering threshold increases from 0.01 to 0.03 g, the mean values increase at increasing distances as magnitude increases relative to the unbiased case, as expected. This effect is only apparent for *M=4-6* at a threshold of 0.01 g, but affects all magnitudes at the 0.05 g threshold at the largest distances (not shown). Note that the strength of this effect is also dependent on the values of the patch distribution mean and sigma. A lower mean increases the threshold effect because more values are below the threshold. A lower sigma, on the other hand, decreases the threshold effect because fewer values are below the threshold when the distribution is narrower.

The effect of the lower-limit threshold is also influenced by the number of allowed resampling attempts required to exceed the threshold. Though we do not show these results, the number of resamples permitted produces several effects. First, as the number of resamples is reduced, the level of the curves is reduced because fewer extremes are sampled. Second, the variance is increased because the mean value plotted may be computed for fewer than 100 stations. That is, some station distances produce only a few exceedances, and some produce none for the given set of parameters. If no exceedances are observed, no value is plotted at that distance. Use of a relatively low number of retrials may produce a result that mimics the actual availability of data at the affected magnitude-distance pairs.

EFFECTS OF PATCH UPPER-LIMIT GROUND MOTION

Setting a finite limit for the ground motion that can be sampled from the patch ground-motion distribution may be justified on the basis of a rock-strength limit. In the past, peak-acceleration limits near 2 g have been suggested (i.e., Brune, 1970) on this basis. Such a limit should have an effect both on level and scaling of our *Z-curves*.

Figure 8d-f shows the effect of limiting the maximum peak acceleration at the patches. The plot with no limit has *log(mean)=0.0* and *log(standard deviation)=0.3*. The values with no upper limit give magnitude scaling and *Z-curve* levels comparable to those observed in the data. Setting the truncation value at 3 g, which is near that suggested in literature, severely reduces both the magnitude scaling and curve levels relative to that of the no-upper-bound case (and, hence, the observations). Although, this result is dependent on the assumed mean and sigma, a higher mean would contract the available range of ground motions to be sampled and, thus, further reduce the magnitude scaling. Ordinarily we would expect a higher value of sigma to expand the scaling and increase the level. In the presence of a 3-g near-field limit, however, the *M 6-8* curves are almost fixed in level, the *M 5* curve moves slightly higher, and the *M 4* curve exhibits lower values

because the number of samples below the mean increases faster than those above the mean. A 3-g upper limit decreases the scaling to a degree that is less than that in the data for *M 6-8*. These results suggest that the upper limit for peak acceleration is higher than previously supposed. This conclusion, however, must be qualified by considering the likely presence of site effects in the data, the treatment of peak-acceleration characteristics in the near-field, and other limitations noted above. We consider these factors in the data fitting and discussion sections below.

STRENGTH OF CRUST VS. DEPTH PARAMETER

Another factor that may control peak-acceleration attenuation is crustal shear strength. For the simulation we assume that the peak acceleration that is generated by a patch at a given depth is proportional to the shear strength of the crust at that depth. This property can be modeled by multiplying the patch peak acceleration by the relative shear strength at the patch depth. The relative shear strength is not known exactly, but several models have been suggested and tested against heat flow measurements. One such model (Turcotte, Tag, and Cooper, 1980) is:

$$\begin{aligned} \tau / \tau_0 &= z / d_1 \qquad z \le d_1 \\ &= e^{(1-(z/d_1)^n} \quad z > d_1 \end{aligned} \tag{1}$$

Typical values of d_1 and n are 14.2 and 1.38, respectively. We expect that this modification should reduce the effective number of patches represented in the extremes and, hence, reduce both curve levels and magnitude scaling. Note that in applying this effect, the patch upper limit, when one is included (see discussion section), is only produced at depth d_1.

Figure 9a shows this function and its effect on the peak-acceleration characteristics and can be directly compared with the no-lower limit panel in figure 8a. Inclusion of the strength function generally reduces the level of the curves, particularly at short distances. This feature results because, at short distances, where the shallow parts of crustal faults tend to be closest to the stations, the strength is low. At large distances, the deeper parts of subduction faults tend to be closest to the stations, but strength is also low. Therefore, for this model of crustal strength, subduction-zone faults tend to produce acceleration-attenuation curves that lie below the crustal $M=8$ curves over a significant range in distance. Stated differently, the part of the fault that is producing the largest peak acceleration is farther away than the closest distance to the fault for most station locations, yet the attenuation distance is the patch-station distance, and the plotting position is the closest distance to the fault. This combination of circumstances leads to lower values for most distances.

Our principal inference from this experiment, however, is that, if crustal strength produces a depth-dependent stress drop, the statistical properties of peak accelerations are significantly influenced. Is such an influence seen in the data? We will address this issue in the discussion section.

Modifying the Model for Data Fitting

Next, we compare model curves with two smoothed data representations determined in the previous study (Perkins, Rogers, and Campbell, in prep.) and described above. For the comparison between model and data, we modify the model to make it more realistic. For example, rupture depths are randomized according to the following rules. For *M 4-5* earthquake rupture depths are randomized so that faults lie randomly between the surface and 10 km. For earthquakes with $M \ge 6$, rupture depths are randomized so that faults lie randomly between the surface and the brittle-ductile boundary (assumed to be 15 km for crustal events and 20 km for subduction events). *M 8*-crustal earthquakes with fixed vertical dip rupture the width of the seismogenic zone, and, therefore, for this case, depths are not adjusted. As before, dip is uniformly randomly distributed in the range $60 \le dip \le 90$ degrees for crustal faults and in the range $10 \le dip \le 20$ degrees for subduction faults.

We also randomized the fault length and width based on observed relationships for rupture area versus magnitude and aspect ratio versus magnitude. Fault length and width were obtained from

empirical relationships for the rupture area and subsurface length (Wells and Coppersmith, 1994). For a given magnitude in the range *M 4-7*, we assumed that the logarithm of the area

$$\log(area) = -3.49 + 0.91M \pm 0.24 \quad (2)$$

is normally distributed with mean and standard deviation given by this equation. The fault length and width were computed from:

$$\begin{aligned} fault\ length &= \sqrt{fault\ area / aspect\ ratio} \\ fault\ width &= fault\ length \times aspect\ ratio \end{aligned} \quad (3)$$

For *M 4-7* earthquakes, the maximum width of faulting, *max.width=15 km/sin(dip)*. If the computed fault width in (3) is greater than *max. width*, the *fault width* was set equal to the *max. width,* and the *fault length = fault area/max. width*. For *M 8*-crustal earthquakes, this procedure occasionally gave lengths that were larger than values reported in the literature, thus, for these earthquakes, we assumed *dip = 90* degrees, *max. width of the fault = 15 km*, and obtain the fault length from

$$\log(fault\ length) = -2.44 + 0.59M \pm 0.16 \quad (4)$$

(Wells and Coppersmith, 1994) . For *M 8*-subduction thrust earthquakes, we compiled fault areas for events ranging between *M 7.8* and *M 8.2* because Wells and Coppersmith's relation is not valid for subduction zone thrust faults. We regressed *log(area[km^2])* against *M* to obtain:

$$\log(area) = -6.11 + 1.27M \pm 0.24 \quad (5)$$

As before, equation (3) was used to obtain the fault dimensions.

Upper and lower limits are also placed on these distributions as shown in Table 1. These limits are approximately equal to the observed limits. Aspect ratios (fault width/fault length) reported in the literature vary widely, especially for subduction thrust earthquakes. The aspect ratios we assume are shown in Table 1. Magnitude 8-crustal ruptures have variable aspect ratios that range between 0.04 and 0.09, values established by the random fault length and fixed maximum width. For *M* 8-subduction ruptures we assume an *aspect ratio=0.75*. Other values of the aspect ratios could have been used without affecting the results substantially, but the values we assume are based on earlier observations (Astiz, Kanamori, and Eissler, 1987; Kasahara, 1981; Scholz, 1982; Thatcher, 1989; Wyss, 1979). The effect of aspect ratio is shown in figure 10, which demonstrates that variation of the aspect ratio by more than an order of magnitude commonly produces less than a 0.1 unit variation in Z (i.e., in *log Ap*).

Table 1. Inclusive limits on fault rupture areas

	Area[km^2]		
Magnitude	Lower Limit	Upper Limit	Aspect Ratio
4	0.5	9	1
5	3	30	1
6	30	250	0.65
7	300	1650	0.33
8-crustal	170 [length: km]	400 [length: km]	variable
8-subduction	6900	40000	0.75

The distributions of fault length and width resulting from these assumptions are shown in figure 11. The results of 100 trials are plotted for each magnitude level. As expected, for *M 4-6*, the distributions for fault width are identical to those for fault length because the aspect ratio assumed is 1 and because the faults are never large enough to exceed the maximum downdip width. The area values for *M 4* are an extrapolation of the relationship of Wells and Coppersmith, and our length and width values are somewhat larger than reported in seismological determinations (i.e., Dysart, Snoke, and Sacks, 1988; Fletcher, Boatwright, and others, 1984; Haar, Fletcher, and Mueller, 1984), which tend to be less than 1 km radius. This discrepancy, however, is not of significance because our model produces only one patch for an *M 4* event when the patch size is 3 km (the value used for most fitting trials) and the aspect ratio is 1. Note that scaling of peak

acceleration for $M<4$ will not occur unless the patch size assumed is smaller than 3 km because in this case only one patch (or partial patch) exists for all smaller magnitudes. This difficulty could be overcome by assuming smaller patch sizes or by assuming that the peak-acceleration distribution mean is magnitude dependent for small magnitudes.

The histogram for *M 7* fault widths is skewed to the high end because most *M 7* events rupture the maximum downdip width. For such events, the aspect ratio is implicitly altered as described above to preserve the fault area. The width distribution for *M 8* ruptures is similar (allowing for a scale change) because these events also rupture the maximum downdip width. In both these cases, the widths are mostly fixed and hence the distribution of lengths resembles the distribution of areas.

Many *M 8* subduction events also rupture the maximum downdip width, which is 143 km for a dip of 10 degrees and 73 km for 20 degrees. As a result, the width distribution concentrates at the shorter width end, with the result that the length distribution resembles that of the area, and the aspect ratio is frequently larger than the assumed value of 0.75.

We use an anelastic attenuation function like that used in past regression studies and given by $Ap \sim Exp[-kr]$. A range of path attenuation values have been used in attempting to fit the data. Although a value of $k=0.0026$, which implies a $Q=150$ at 1 Hz, has been used in several studies of peak-acceleration attenuation (Campbell, 1987; Joyner and Fumal, 1985), we found that $k=0.0013$ best fit our smoothed data representations on average. As noted below, however, we concluded that a magnitude dependent k-value was suggested by the data.

Panels a, b, and c in figure 12 compare model results with the smoothed data for several patch lengths. Panel a, with a patch length of 3 km and a mean patch acceleration of 0.9 g produces a fit that is very similar to that of panel b, with a patch length of 1 km and a mean patch acceleration of 0.4 g. Sigma has been adjusted only slightly. We found, after comparing a variety of model results with the data, that there is a range of model patch size-mean pairs which fit the data. Smaller means require smaller patch sizes. Panel c presents a fit for patch size 0.5 km with a mean of 0.3 g, and shows the relatively wide range of patch size-mean pairs that can approximate the data. A patch size of 3 km (panel a) appears to achieve a marginally better fit. Furthermore, we found that a patch size of 3 km combined with a relatively larger mean produces values above the threshold for *M 6* at large distance more readily than does a smaller patch size with a relatively smaller mean. Thus, a patch size of 3 km is also preferred on this basis because this result is more nearly like the data attributes (i.e., values above the threshold at large distance for *M 6*).

Panels a and d compare model predictions for two values of patch acceleration standard deviation, sigma, while holding patch size fixed at 3 km. Although panel d does not show as good a fit for the lower magnitudes, we can observe that sigma and the mean anticorrelate for model predictions that approximate data. Hence, our model cannot discriminate between a range of sigma-mean pairs in which sigma and mean anticorrelate. The ranges in mean and sigma, however, given a fixed patch size, are limited by two factors. Given a patch size of 3 km, values of the mean larger than about 1.0 g push the levels of the curves higher than the observations, though this effect can be partially offset by smaller values of sigma. But as sigma decreases, magnitude scaling (da_p/dM) becomes less than observed. Conversely, values of the mean less than 0.2 g require increasing sigma, but this change creates magnitude scaling that is larger than required. Thus, once the patch size is set, the range of acceptable mean-sigma pairs is restricted.

The other parameters in the model produce secondary effects, and we adjusted these after seeking values of the mean and sigma for a fixed patch size. No upper bound on the patch-acceleration distribution was used in fitting the data because the upper limit compresses the magnitude scaling for magnitudes *M 7-8* in a manner not present in the data. A triggering threshold in the range of 0.01 to 0.03g fits the data best. Higher values produce too much sampling bias, and lower values do not produce enough bias.

The comparison shown in figure 12 suggests possible modifications of the model. For example, the model curve appears to be too high for the *M 8* data beyond about 30 km. Although partially masked by triggering bias, the model curve appears too high for the *M 7* data when

$\log R > 1.7$ and for the *M 6* data when $\log R > 1.5$. The *M 4-5* ground motions do not trigger at the large distances displayed by the predicted ground motions, which implies that the model attenuation (k) for these magnitudes is too low. Hence, these comparisons suggest that the attenuation operator is likely to be magnitude dependent. Magnitude-dependent attenuation is plausible because, at a given distance, the data indicate that peak-acceleration predominant period increases with increasing magnitude (Gutenberg and Richter, 1942; Gutenberg and Richter, 1956). Inasmuch as $k \propto 1/(TQ(T))$, k may be a function of period (T), and the appropriate value of k for peak acceleration may be a decreasing function of magnitude. Below, we modify the model to include magnitude dependent k-values.

Other explanations for the *M 8* discrepancy are possible. First, the smoothed values for *M 8* are based on sparse data. The *M 8* data values for *R>30 km* are too variable and too few to constrain the data smoothing (Perkins, Rogers, and Campbell, in prep.). When another smoothing technique using paradigmatic shapes is applied (Perkins, Rogers, and Campbell, in prep.), the level of the peak on *M 8* is reduced and the peak on *M 5* disappears. Second, we expect that *M 8* events present the greatest likelihood to produce time addition of pulses at distant stations because of isochrone effects and possible magnitude-dependent patch sizes, thus violating one of the assumptions of the extremal model. Third, the data base is known to contain site effects not yet included in the model, and these effects may be distance dependent (Rogers, Perkins, and others, 1991). Hence, in the following, we explore this question. Is it possible to apply distance-dependent site effects and magnitude-dependent attenuation to the model in order to obtain better correlation with the data?

First, we examine the effects of these changes to the model in figure 13. Figure 13a-c compares the cases: no site effect, constant site effect, and distance-dependent site effect. Constant site effect is a factor of two at all distances. The distance-dependent site effect applied is a tripartite continuous linear function with log-normal variability (standard deviation=0.3 and upper and lower distribution bounds given by $mean \log(site\ factor) \pm 0.5$), where site factor is given in table 2. This site function is similar to that found in an earlier study for soft-soil sites (Rogers, Perkins, and others, 1991).

Table 2. Distance dependent site factors assumed.

R (km)	Mean Log(site factor)
2.5	0.30
7.9	0.32
25	0.34
>79	0.54

Figure 13 panels a and b (or c and d) compare the effect of assuming attenuation is magnitude dependent while holding the site effect constant. Magnitude-dependent attenuation permits sampling bias to truncate the curves at distances that increase with magnitude, an effect that is stronger than observed in the results of figure 12, but is more in line with the data characteristics. Finally, panel f shows the results when both distance-dependent site effects and magnitude-dependent attenuation are included. This fit to the data is best for *M 6-8*. The underestimate for *M 5* could be due to too much anelastic attenuation in the model. This comparison is not intended to represent a tuned fit but shows that improved fitting of the data is possible with these model changes.

FITTING BOTH SMOOTHED DATA REPRESENTATIONS

In the following, we attempt to fit the smoothed data and paradigm data simultaneously. If the smoothed data with bias can be fit by model parameters with bias, then the paradigm data, which minimize sampling bias, should be fit by the same parameters, but with a small or no lower limit to minimize sampling bias in the model results. Note that sampling bias will always be present to some extent because our treatment of the paradigm data only marginally extrapolates the data below the threshold. Thus, there is always some level below which no data exist; that is, no stations

trigger and there is no basis for extrapolation. This fact is difficult to simulate exactly in the model, but we assume a value of the triggering threshold of 0.005 g as an approximate treatment.

Figure 14 shows several attempts to fit both data representations. These results are drawn from a set of trials that used means ranging from 0.4 g to 1.1 g in steps of 0.1 g and sigma ranging from 0.2 to 0.45 in steps of 0.0275. In these trials, we assumed distance-dependent site effects and magnitude-dependent attenuation as discussed above. The data-model comparisons for the lowest value of the mean (0.5 g) for which the fit begins to be acceptable are shown in figures 14a and b. The fit to the smoothed data (panel a), however, is a better fit than that to the paradigm data (panel b), which tends to underestimate *M4-6*. Panels c and d show our best effort to fit both data representations from our set of trials without further tuning of the model parameters. The site effect of the size assumed is not large enough to fit the *M8*-subduction data. Thus, the site effect is bigger than we estimate, and or the limitations of the model discussed above must play a role.

Panels e and f show that as the patch mean increases beyond 0.8 g the fit to the data becomes poorer, particularly at close-in distances for *M4-5*. As the mean increases beyond 1 g, the quality of the fit disintegrates for both data representations and all values of sigma. Although further tuning of the parameters around those for panels c and d would undoubtedly achieve improved fitting of the data, we only wish to demonstrate that the model is capable of reproducing much of the complex data attributes under fairly simple assumptions.

FITTING THE DATA WITH A PATCH-ACCELERATION UPPER LIMIT AND A STRENGTH OF CRUST EFFECT

Here we address the following question: Do the data also require a patch-acceleration upper limit and (or) a strength-of-crust effect? In figures 15a and b we show the effect of inclusion of upper limits of 3 g and 5 g. Panel b shows that a fit can be obtained with a 5 g limit that is very similar to that obtained with no upper limit (compare with figure 14d). The curves with the 5 g limit are only marginally reduced in level. The 3 g limit is more severe and degrades the fit substantially, although it might be improved by increasing the sigma value. We conclude the data do not require an upper limit, but inclusion of a limit greater than 3 g does not prevent us from fitting the data.

Figure 15 c and d show attempts to fit the data including both the crustal-strength function and an upper limit. Fitting of the data requires a doubling of the mean patch acceleration and reduction of sigma to approximate a fit. The strength function produces several other effects. First, note that the *M8* subduction case is lowered at distances for $log\ R<1.4$, a result that does seem more in accord with the data characteristics. It also results in *M8* subduction earthquake ground motions that are lower than the crustal *M8* events at some distances. This result, in fact, may be present in the data (Perkins, Rogers, and Campbell, in prep., figure 8) represented in magnitude slices. It does not appear in our distance slice results because the smoothing function used minimized this attribute. Hence, we believe this aspect of the model may in fact be present in the data. The fit obtained by including the crustal strength function, however, is generally poorer than the results without it. The fit could be improved in this case by increasing anelastic attenuation for *M4-6*. Whether the data require the crustal-strength modification and upper limit is unclear, but it is possible to fit the data while incorporating them in the model, as demonstrated by figure 15.

Discussion

The motivation for this study was the realization that no model or empirical functional form fully described the observed scaling characteristics of peak acceleration with magnitude and distance (figure 1a). For example, while mean observed peak accelerations increase with increasing magnitude, the rate of increase declines with magnitude at distances less than 30 km and increases for M6-8 between 30 and 80 km. Beyond 100 km the curves converge. These features have not been predicted by most stochastic and regression earthquake ground-motion models.

Furthermore, in regression studies, it is difficult to select among functional forms because the data are highly variable. A standard functional form for peak-acceleration regression has not been universally accepted (Bolt and Abrahamson, 1982; Bolt and Abrahamson, 1983; Brillinger and

Preisler, 1984; Brillinger and Preisler, 1985; Joyner and Boore, 1983). Presumably the best functional form is one that is based on the physics of the source, path, and site; yet, it is likely that, even with a functional form based on physics, the data applied to that form may be affected by data sampling effects that are not explicitly expressed by the regression model. As we have shown, such statistical effects mask the relationship between the data and the physical parameters expected to predict the data characteristics. A functional form, based solely on physics, that is fit to a data set containing variable-dependent statistical effects can only be fit effectively, if the effects are removed, minimized, or included as part of the fitting model.

Our model contrasts with earlier stochastic models in several ways–principally because we achieve scaling of peak acceleration without time addition of pulses at the station or scaling of peak acceleration at the source. In some stochastic models, magnitude scaling of peak accelerations is produced by the statistical time addition of pulses that arrive at the recording site randomly and by the increased likelihood of such addition as the rupture duration increases (i.e., Boatwright, 1982; Boore, 1983). Other stochastic models add subevent spectra with random phase (i.e., Andrews, 1981; Frankel, 1991), a method that implicitly assumes time addition of pulses. Random addition of pulses, however, may not be required to model peak-acceleration characteristics because short-duration wide-bandwidth pulses generated by a propagating short-rise-time rupture may not overlap in a manner that is strongly dependent on fault size (Cocco and Boatwright, 1993). The scaling in our model is produced solely by finite-fault geometry, by stochastic properties of the patch accelerations, and by sampling of extremes resulting from interaction of these two factors.

Most earthquake source models predict relatively simple peak-acceleration functional dependence on magnitude and distance. For example, predicted peak-acceleration scaling with earthquake size ranges from no scaling (i.e., Hanks and Johnson, 1976) to M_0^n, where M_0 is the seismic moment and n is a constant with values between *1/3* to *1/6* (i.e., Boore, 1983; McGarr, 1984). The scaling of peak acceleration with earthquake size according to such simple functional forms does not appear to be supported by the data. Our model produces complex peak-acceleration characteristics in response to varying earthquake size and distance that fit the data..

Recent modeling of ground motions (see, for example, Heaton, 1990, for a review) suggests that the slip-rise time is much shorter than the duration of fault rupture. Furthermore, the slip-rise time may increase with increasing magnitude. This result is consistent with the concept of fault patches but with a magnitude-dependent patch size. In view of widely observed earthquake characteristics such as ω^{-2} spectral decay and *b-value=1,* which both suggest self-similar rupture (i.e., Andrews, 1980; Andrews, 1981; Frankel, 1991; Hanks, 1979), a patch size proportional to fault radius is a different and possibly more appropriate assumption than our assumed constant patch size. With most fractal models, however, the number of patches increases with magnitude. We note that a patch area that increases in proportion to fault area would not produce acceleration scaling in the extremal model, unless the proportionality was such that $patch\ area \sim (fault\ area)^n$, where $n < 1.$, or unless the patch mean scaled with magnitude. That is, if $n = 1$, all fault lengths have the same number of patches. If, however, $0 < n < 1$, the number of patches again increases with fault length and peak-acceleration scaling will occur. For values of n approaching 1, however, sigma would have to increase to achieve scaling comparable to that associated with smaller values of n. Alternately, if n=1, scaling could still exist, if the peak-acceleration mean is also proportional to patch size/magnitude. Note, however, that the scaling in this case would not be distance dependent. The attenuation curves at all distances would be offset a constant amount, a result that appears contrary to that observed in the peak-acceleration data. Another possibility, so far untested in this model, is the incorporation of a fractile patch size distribution, as has been proposed by some (i.e., Frankel, 1991).

Nonetheless, our model incorporates several significant features of self-similar rupture models: (1) a statistically randomized dynamic stress drop with constant mean and (2) an increasing number of patches with increasing fault size. Our treatment of the dynamic stress drop may serve as an adequate proxy for the actual case in modeling peak values, though it does not include the fractile spatial distribution of patches expected in self-similar rupture models.

Our model, as implemented, can not predict spectral characteristics even though we expect extremal effects to influence spectra. We would argue that the sampling-of-extremes aspect of this model would influence spectra because a time series with a larger peaks due to increased numbers of patches will have a higher spectral level than one with a lower peaks due to fewer patches. Thus, this model, had it included Green's functions, would have resulted in spectral scaling with earthquake size because of the statistical distribution imposed on the peak values of the Green's functions. Our argument intuitively suggests, moreover, that we could model the scaling properties of spectra for faults with self-similar rupture characteristics by requiring separate distributions on the peak and period of the patch Green's function. These distributions would proxy for the patch size dependency on magnitude. Thus, the sampling of extremes property must be a first-order effect of both peak values and spectra, though this characteristic is no doubt superimposed on other effects, such as the time addition of pulses for some rupture styles and station positions relative to the fault. Further, exploration of this idea is beyond the scope of this study.

The results of this model study suggest that peak-acceleration characteristics are more complex than recognized in earlier regression studies that have commonly assumed regression function forms incapable of expressing the characteristics we have modeled. Our model results could be used to develop new regression functional forms that would properly represent peak-acceleration characteristics. Such an effort would require addressing what is to be fit. If one wishes to fit the data with sampling bias included, the functional form for the model must include the capability to simulate this bias. In using the model for predictions, however, the bias term would presumably be removed. All these issues are beyond the scope of this study.

Conclusions

We have shown that a finite-fault Monte-Carlo earthquake source composed of uniformly distributed patches having constant statistical properties approximates observed scaling characteristics of peak accelerations as a function of magnitude and distance. If a lower-limit detection threshold is included, this model produces sampling bias effects, which are also noted in the data. These model results are in accord with smooth data representations from an earlier study (Perkins, Rogers, and Campbell, in prep.) that are based on an undifferentiated worldwide data set spanning magnitudes 4-8, including both crustal and subduction earthquakes.

The primary parameters in this model are the mean and standard deviation of a log-normal distribution that specifies patch acceleration sampling, patch size, and accelerometer triggering threshold. A parameter variation study indicates that either patch size or distribution mean must be assumed in fitting the data because the effects of mean and patch size are roughly interchangeable. For example, the mean required to fit the data with a 3 km patch size is about twice that required with a 1 km patch size. Our fitting of the data constrains the standard deviation of the patch distribution to lie in the range 0.2-0.4 (units of log g). For the most part, neither the data nor the model support maximum near-field site accelerations that are low (less than 3 g, though not well established).

We also found that the triggering threshold required to fit the data is in the range 0.01 to 0.02 g, as might be expected from a cursory examination of the data base. This detection threshold produces bias in acceleration attenuation at varying distances for M 4-7. The existence of bias over this range of magnitudes was not anticipated. The best data and model comparisons also require magnitude-dependent anelastic attenuation and distance- or magnitude-dependent site effects.

Notwithstanding the model's simplifying assumptions, its capacity to approximate complex peak-acceleration features suggests that much of the statistical and physical process governing peak-acceleration attenuation is represented. The statistical effects produced by the model include the special scaling properties that we term distance-dependent magnitude saturation and triggering bias. These effects are not represented in earlier stochastic models. Both the model and the data also suggest that more complex regression models than have commonly been used in the past are required to fit the data. Regression functional forms should accommodate distance-dependent magnitude saturation, triggering bias effects, site effects, and possibly magnitude-dependent anelastic attenuation.

Our results could be used to develop new regression functional forms that would properly represent peak-acceleration features. Such an effort would require addressing what is to be fit. If one wishes to fit the data with sampling bias included, the functional form for the model must include the capability to simulate this bias. In using the model for predictions, however, the bias term would be removed. On the other hand, the prediction of peak acceleration might be best accomplished by empirical, smoothed representations of the data in graphs or tables that have the sampling bias minimized, as in our earlier study (Perkins, Rogers, and Campbell, in prep.).

Acknowledgments

We thank Arthur D. Frankel and Stephen H. Hartzell for their helpful reviews of this manuscript.

References

Andrews, D.J., 1980, A stochastic fault model 1. static case: Journal of Geophysical Research, v. 85, no. b7, p. 3867-3877.

Andrews, D.J., 1981, A stochastic fault model 2. time-dependent case: Journal of Geophysical Research, v. 86, no. B11, p. 10821-10834.

Astiz, L., Kanamori, H., and Eissler, H., 1987, Source characteristics of earthquakes in the Michoacan seismic gap in Mexico: Seism. Soc. Am. Bull., v. 77, no. 4, p. 1326-1346.

Bernard, P., and Madariaga, R., 1984, A new asymptotic method for the modeling of near-field accelerograms: Seism. Soc. Am. Bull., v. 74, no. 2, p. 539-557.

Boatwright, J., 1982, A dynamic model for far-field acceleration: Seism. Soc. Am. Bull., v. 72, no. 4, p. 1049-1068.

Boatwright, J., and Quin, H., 1986, The seismic radiation from a 3-D dynamic model of a complex rupture process, Part 1: Confined ruptures, Washington, D.C., American Geophysical Union, p. 97-109.

Bolt, B.A., and Abrahamson, N.A., 1982, New attenuation relations for peak and expected accelerations of strong ground motion: Seism. Soc. Am. Bull., v. 72, no. 6A, p. 2307-2321.

Bolt, B.A., and Abrahamson, N.A., 1983, Reply to W.B. Joyner and D.M. Boore's "comments on 'New attenuation relations for peak and expected accelerations of strong ground motion'": Seism. Soc. Am. Bull., v. 73, no. 5, p. 1481-1483.

Boore, D.M., 1983, Stochastic simulation of high-frequency ground motions based on seismological models of the radiated spectra: Seism. Soc. Am. Bull., v. 73, no. 6, p. 1865-1894.

Brillinger, D.R., and Preisler, H.K., 1984, An exploratory analysis of the Joyner-Boore attenuation data: Seism. Soc. Am. Bull., v. 74, no. 4, p. 1411-1450.

Brillinger, D.R., and Preisler, H.K., 1985, Further analysis of the Joyner-Boore attenuation data: Seism. Soc. Am. Bull., v. 75, no. 2, p. 611-614.

Brune, J.N., 1970, Tectonic stress and the spectra of seismic shear waves from earthquakes: Journal of Geophysical Research, v. 75, no. 26, p. 4997-5009.

Bury, K.V., 1975, Statistical Models in Applied Science: New York, John Wiley & Sons, 625 p.

Campbell, K.W., 1985, Strong motion attenuation relations: a ten-year perspective: Earthquake Spectra, v. 1, no. 4, p. 759-804.

Campbell, K.W., 1987, Predicting strong ground motion in Utah, *in* Hays, W.W., and Gori, P.L., eds., eds.: U.S. Geological Survey Open-File Report 87-585, p. L1-L90.

Cocco, M., and Boatwright, J., 1993, The envelopes of acceleration time histories: Seism. Soc. Am. Bull., v. 83, no. 4, p. 1095-1114.

Dysart, P.S., Snoke, J.A., and Sacks, I.S., 1988, Source parameters and scaling relations for small earthquakes in the Matsushiro region, southwest Honshu, Japan: Seism. Soc. Am. Bull., v. 78, no. 2, p. 571-589.

Fletcher, J.B., Boatwright, J., Haar, L.C., Hanks, T.C., and McGarr, A., 1984, Source parameters for aftershocks of the Oroville, California, Earthquake: Seism. Soc. Am. Bull., v. 74, no. 4, p. 1101-1123.

Frankel, A., 1991, High-frequency spectral falloff of earthquakes, fractal dimension of complex rupture, b-value, and the scaling of strength on faults: Journal of Geophysical Research, v. 96, no. B4, p. 6291-6302.

Gutenberg, B., and Richter, C.F., 1942, Earthquake magnitude, intensity, energy, and acceleration: Seism. Soc. Am. Bull., v. 32, no. 3, p. 163-191.

Gutenberg, B., and Richter, C.F., 1956, Earthquake magnitude, intensity, energy, and acceleration: Seism. Soc. Am. Bull., v. 46, no. 2, p. 105-145.

Haar, L.C., Fletcher, J.B., and Mueller, C.S., 1984, The 1982 Enola, Arkansas, swarm and scaling of ground motion in the eastern United States: Seism. Soc. Am. Bull., v. 74, no. 6, p. 2463-2482.

Hanks, T.C., 1979, b values, and $\omega^{-\gamma}$ seismic source models: Implications for tectonic stress variations along active crustal fault zones and the estimation of high-frequency strong ground motion: Journal of Geophysical Research, v. 84, no. B5, p. 2215-2242.
Hanks, T.C., and Johnson, D.A., 1976, Geophysical Assessment of Peak Accelerations: Seism. Soc. Am. Bull., v. 66, no. 3, p. 959-968.
Heaton, T.H., 1990, Evidence for and implications of self-healing pulses of slip in earthquake rupture: Physics of the Earth and Planetary Interiors, v. 64, p. 1-20.
Joyner, W.B., and Boore, D.M., 1983, Comments on "New attenuation relations for peak and expected accelerations of strong ground motion," by B.A. Bolt and N.A. Abrahamson: Seism. Soc. Am. Bull., v. 73, no. 5, p. 1479-1480.
Joyner, W.B., Campbell, K.W., and Harmsen, S.C., 1988, Near-source simulation of earthquake ground motion based on the stochastic omega-square model [abs.]: Seismological Research Letters, v. 59, no. 1, p. 10.
Joyner, W.B., and Fumal, T.E., 1985, Predictive mapping of earthquake ground motion, *in* Ziony, J.I., ed., ed.: U.S. Geological Survey Professional Paper 1360, p. 203-220.
Kasahara, K., 1981, Earthquake Mechanics: Cambridge, Cambridge University Press, 248 p.
Madariaga, R., 1977, High-frequency radiation from crack (stress drop) models of earthquake faulting: Geophys. J., v. 51, p. 625-651.
McGarr, A., 1984, Scaling of Ground Motion Parameters, State of Stress, and Focal Depth: Journal of Geophysical Research, v. 89, no. B8, p. 6969-6979.
McLain, D.H., 1974, Drawing contours from arbitrary data points: The Computer Journal, v. 17, no. 4, p. 318-324.
McLaughlin, K.L., 1991, Maximum likelihood estimation of strong-motion attenuation relationships: Spectra, v. 7, no. 2, p. 267-279.
Perkins, D.M., Rogers, A.M., and Campbell, K.W., in prep., Limitations of the world-wide strong-motion data base: Effects on peak-acceleration regression analyses: U.S. Geological Survey Open-File Report.
Rogers, A.M., and Perkins, D.M., 1994, Peak-acceleration scaling produced by isochron pulse addition and extreme sampling: American Geophysical Union Transactions, v. 75, no. 44, p. 448.
Rogers, A.M., Perkins, D.M., Hampson, D.B., and Campbell, K.W., 1991, Investigations of peak acceleration data for site effects, Oakland, Calif., Earthquake Engineering Research Institute, p. 229-236.
Saikia, C.K., 1994, Modeling of strong ground motions from the 16 September 1978 Tabas, Iran, earthquake: Seism. Soc. Am. Bull., v. 84, no. 1, p. 31-46.
Scholz, C.H., 1982, Scaling laws for large earthquakes: Consequences for physical models: Seism. Soc. Am. Bull., v. 72, no. 1, p. 1-14.
Silva, W., Roblee, C., and Abrahamson, N., 1995, Nonlinear site response during the January 17, 1994 M 6.7 Northridge earthquake: unpub. manuscript, Pacific Engineering and Analysis.
Somerville, P., Sen, M., and Cohee, B., 1991, Simulation of strong ground motions recorded during the 1985 Michoacan, Mexico and Valparaizo, Chile earthquakes: Seism. Soc. Am. Bull., v. 81, no. 1, p. 1-27.
Spudich, P., and Cranswick, E., 1984, Direct observation of rupture propagation during the 1979 Imperial Valley earthquake using a short baseline accelerometer array: Seism. Soc. Am. Bull., v. 74, no. 6, p. 2063-2114.
Spudich, P., and Frazer, N.L., 1984, Use of ray theory to calculate high-frequency radiation from earthquake sources having spatially variable rupture and stress drop: Seism. Soc. Am. Bull., v. 74, no. 1, p. 2061-2083.
Thatcher, W., 1989, Earthquake recurrence and risk assessment in circum-Pacific seismic gaps: Nature, v. 341, no. 5 October, p. 432-434.

Turcotte, D.L., Tag, P.H., and Cooper, R.F., 1980, A steady state model for the distribution of stress and temperature on the San Andreas fault: Journal of Geophysical Research, v. 85, no. B11, p. 6224-6230.

Wells, D.L., and Coppersmith, K.J., 1994, New empirical relationships among magnitude, rupture length, rupture width, rupture area, and surface displacement: Seism. Soc. Am. Bull., v. 48, no. 4, p. 974-1002.

Wyss, M., 1979, Estimating maximum expectable magnitude of earthquakes from fault dimensions: Geology, v. 7, p. 336-340.

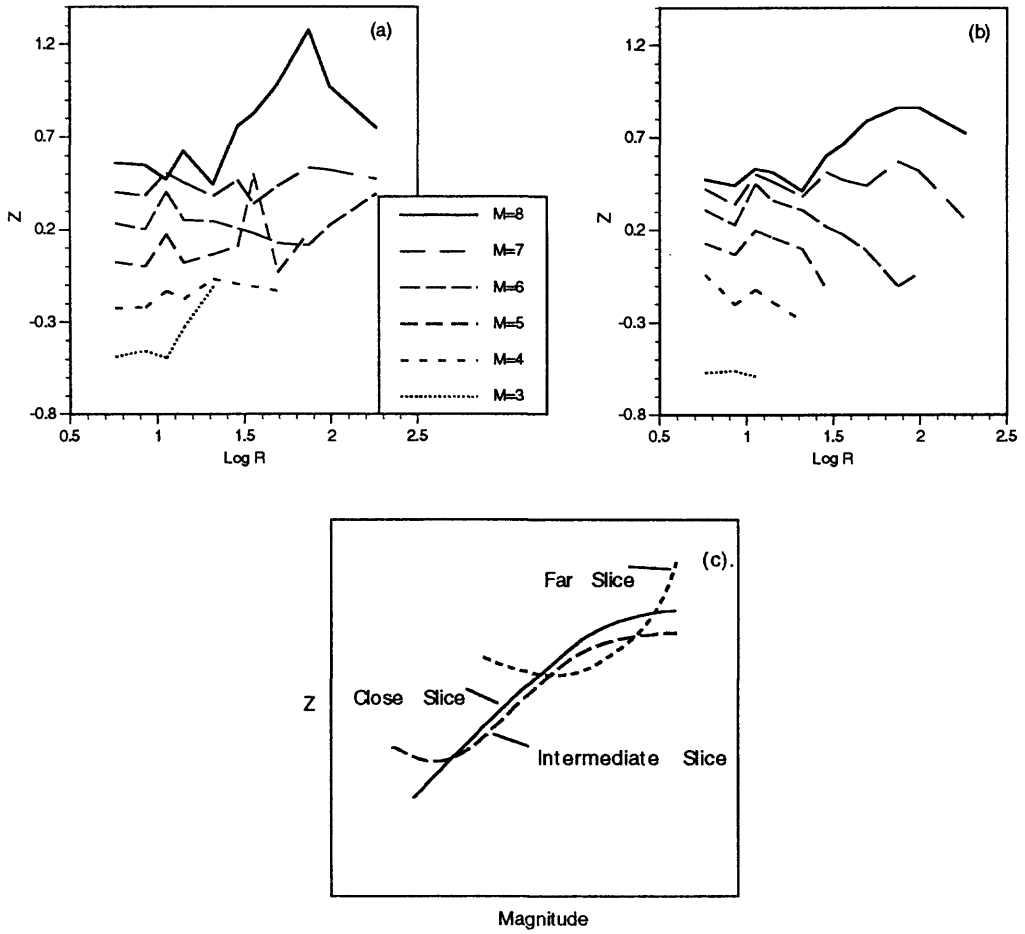

Figure 1. (a). Non-parametric smooth representations of peak accelerations (see the text) based on an undifferentiated worldwide data set (Campbell, written comm., 1990). (b) This alternate version of the data, which is intended to minimize sampling bias produced by instrumental triggering threshold, we term the paradigm data. Both data representations suggest distance-dependent magnitude scaling, and both demonstrate magnitude saturation at distances less than 25 km. (c) This plot shows three idealized smoothed curve fits to the peak acceleration data in narrow distances slices. The close slice is typical of the data at distances less than about 12 km; the intermediate slice is typical of data in the range $12 < R < 25$ km; the far slice is typical of data at distances beyond 25 km. The far and intermediate distance slices demonstrate the effect of sampling bias for large magnitude and small magnitude data, respectively, as indicated by the "j-shape" in the curves for the smallest magnitudes in the slice. The intermediate slice shows sampling bias at small magnitudes. Both the intermediate and close slices suggest magnitude saturation (rollover) as magnitude increases. The close slice has the characteristics we believe are representative of the data with minimal sampling bias. This shape was subjectively fit to the data in all distance slices to minimize sampling bias on the other slices, and the resulting curves were used to produce the paradigm data representation in plot (b).

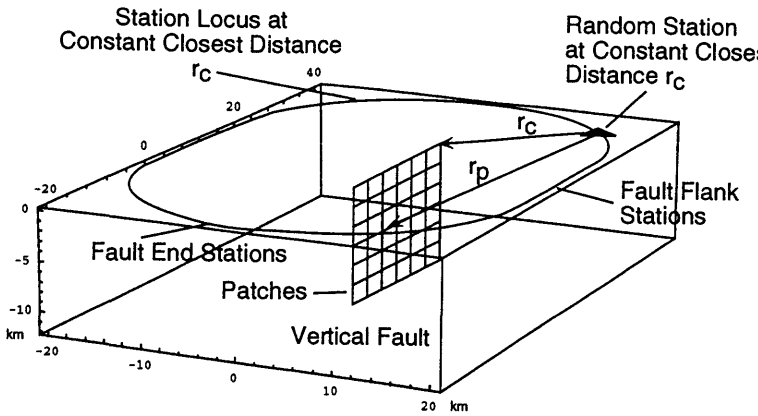

Figure 2. Typical station-source geometry. The fault is composed of patches that produce peak accelerations drawn from a statistical distribution. For the Monte Carlo estimates, stations are randomly selected on the locus of constant closest distance from the fault. Although we show a vertical fault, fault dip is random as explained in the text. In the case of subduction earthquakes, stations are assumed to exist only along the downdip (onshore) fault flank.

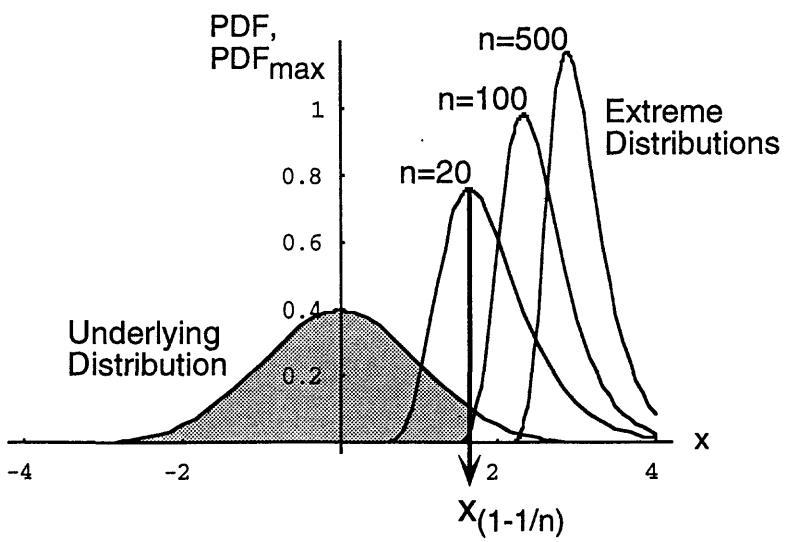

Figure 3. Behavior of Gumbel Type I extreme value distributions as a function of sample size n. In a sample of size n, one random variable value (x) on average is expected to exceed the mode of the extreme distribution, which is located at $x_{(1-1/n)}$, the value corresponding to the $(1-1/n)$ fractile. Hence, as the sample size increases, the mode of the extreme distribution increases and, thus, the likelihood of observing extremes of increasing value increases. In this model, the sample size corresponds to the number of patches of a fault rupture.

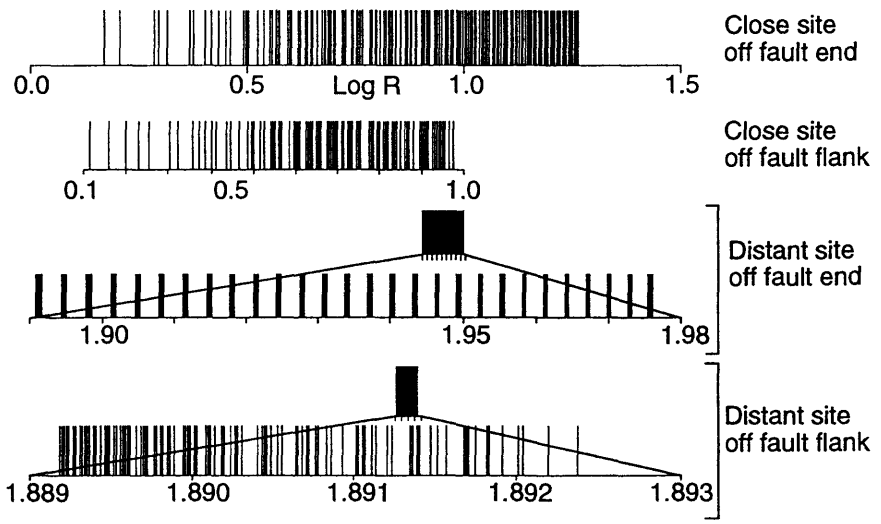

Figure 4. Distribution of patch distances to a station for a fault having 224 patches. For the purpose of demonstrating the distribution properties, two station distances are considered, 2.5 km and 250 km from the fault. For each distance, we show the distribution for sites off the fault flank and off the fault end. The third and fourth panels in this figure are plotted first at the same scale as the first two panels (approximately) and then expanded to show the details. Closely-spaced patch distances indicate the effective number of patches contributing to station ground-motion extremes.

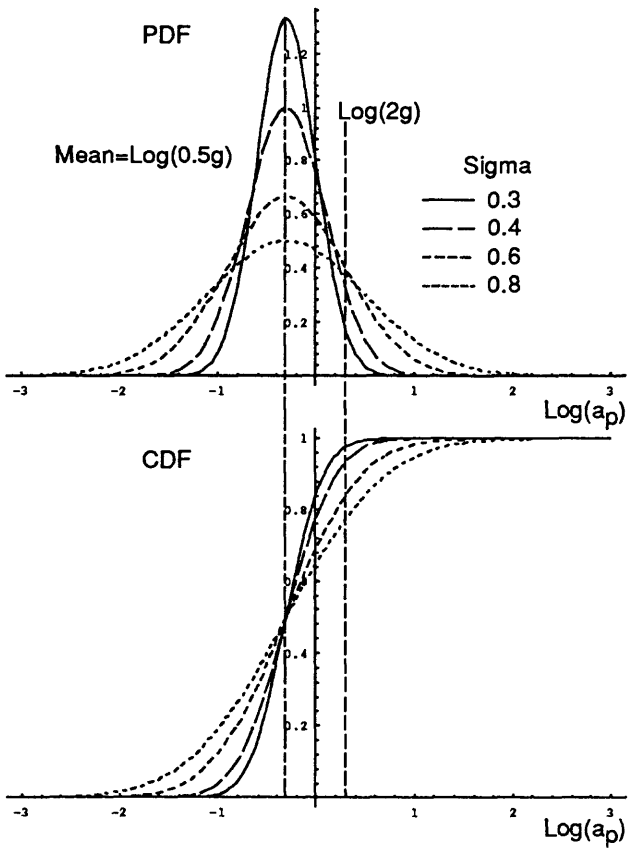

Figure 5. Probability density function (PDF) and cumulative density (CDF) functions for several values of sigma (the distribution standard deviation). The distribution mean assumed is -0.3 (log 0.5 g). The CDF shows the relative likelihood of observing values larger than 2 g for each assumed sigma and this fixed value of the mean.

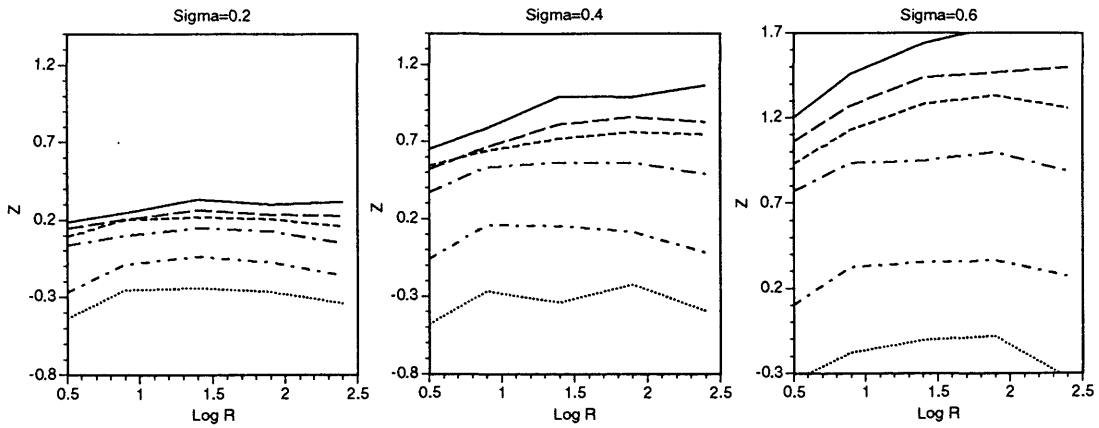

Figure 6. Normalized peak acceleration (Z) as a function of log distance showing the effect of sigma on the scaling of peak accelerations with magnitude and distance. Sigma has a very strong effect on scaling because it controls the sampling of extremes relative to the mean. The solid line is M=8 for a subduction zone earthquake; the lines below are successively M=8 (long dash) through 4 (dotted) for crustal earthquakes. The following parameters were assumed: mean patch peak acceleration=1 g; patch size=2 km; no upper or lower limits; no anelastic attenuation.

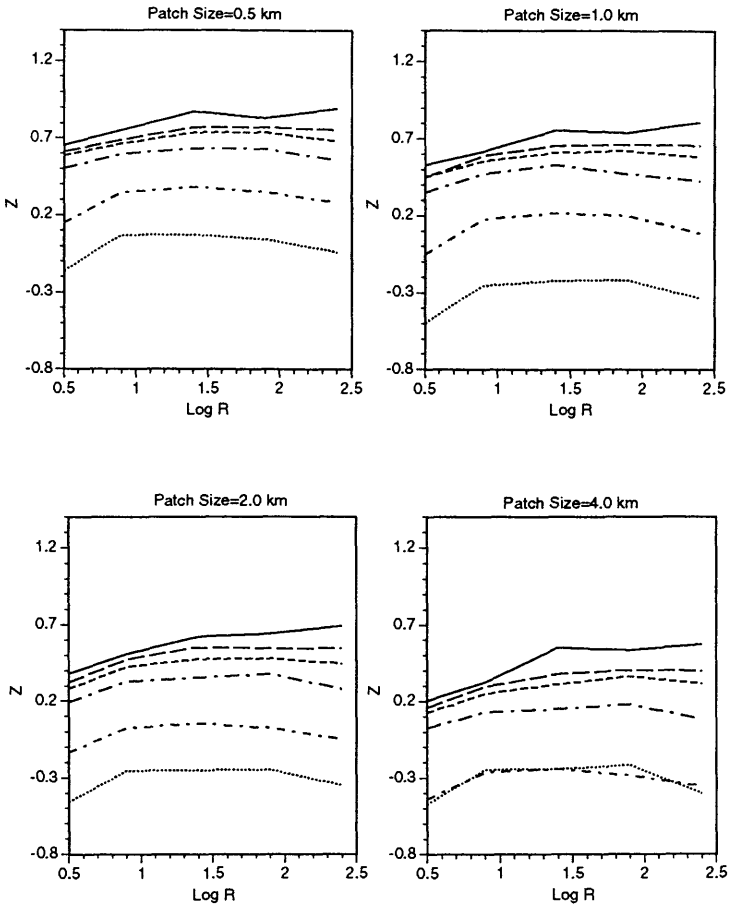

Figure 7 Effect of varying patch size on the characteristics of peak acceleration. Patch size has a strong inverse effect on the level of the curves because as the patch size increases the number of patches decreases. The effect of patch size on magnitude scaling is complex (see text). Curve identifications are as in figure 6. The following parameters were assumed: mean patch peak acceleration=1 g; sigma=0.3; no upper or lower limits; no anelastic attenuation.

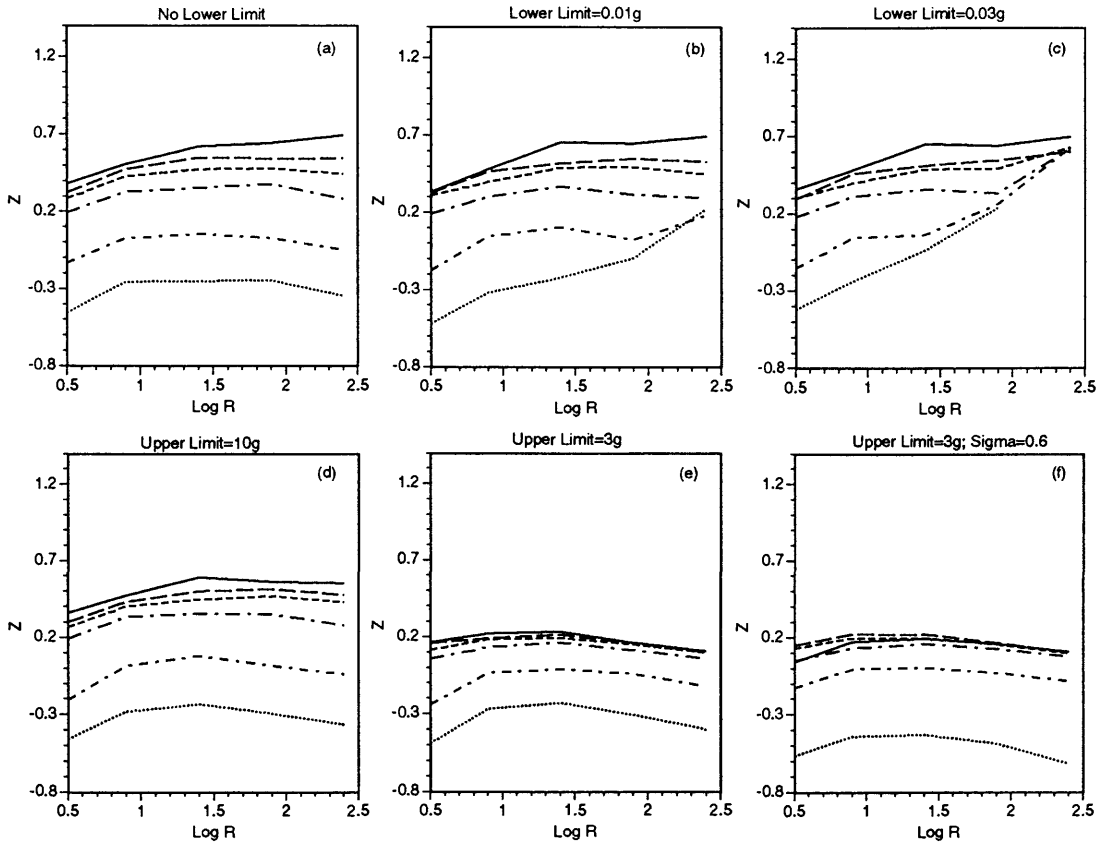

Figure 8 Effect of lower-limit threshold in the upper three panels (a-c) and upper-limit threshold in the lower three panels (d-f) (see text for explanation). Curve identifications are as in figure 6. The following parameters were assumed: mean patch peak acceleration=1 g; sigma=0.3 (0.6 in panel f); no upper limit (1-c, lower limits as shown); no lower limit (d-f, upper limits as shown); no anelastic attenuation. Values are not plotted if no exceedance of the threshold occurs after 200 retries (see the text).

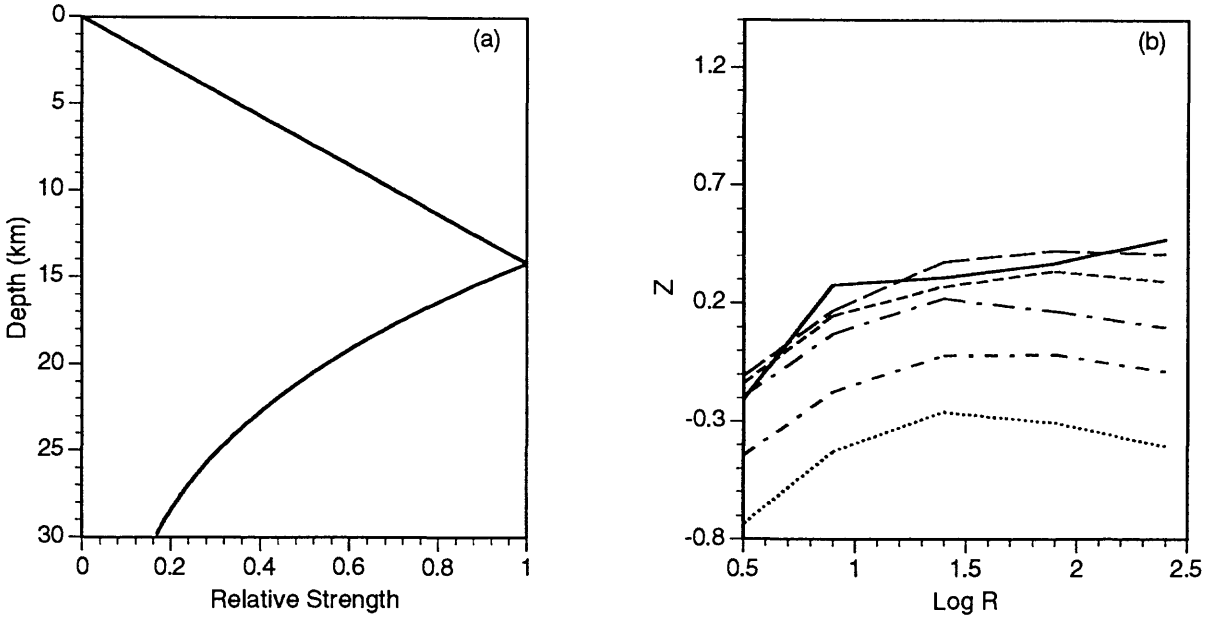

Figure 9 (a). Relative strength function (see text) plotted as a function of depth. (b). Effect of a strength of crust assumption (see text) on peak acceleration characteristics (see text for a discussion). Curve identifications are as in figure 6. The following parameters were assumed: mean patch peak acceleration=1 g; sigma=0.3; no lower limit; no upper limit; no anelastic attenuation.

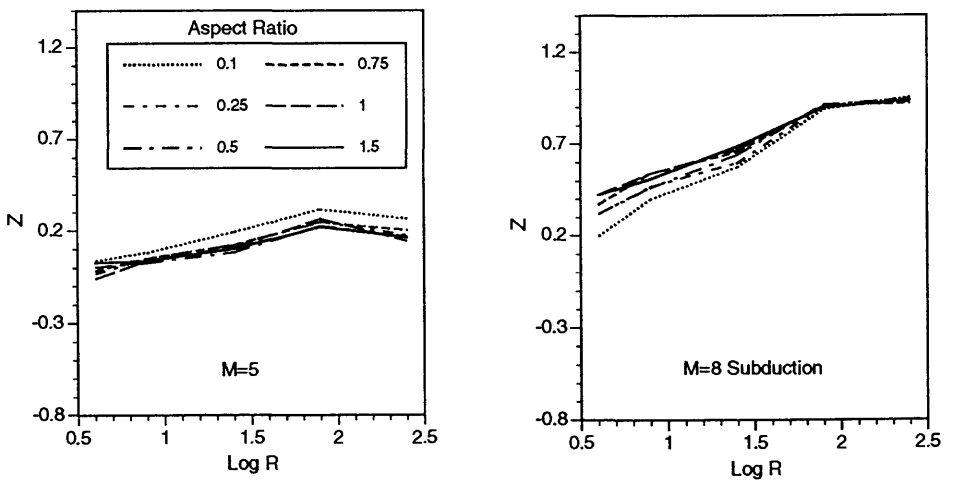

Figure 10 Effect on the scaling behavior of peak acceleration resulting from variation of the fault-aspect ratio (width/fault length) for two earthquake sizes. The results show the aspect ratio produces effects commonly less than 0.1 units in Z.

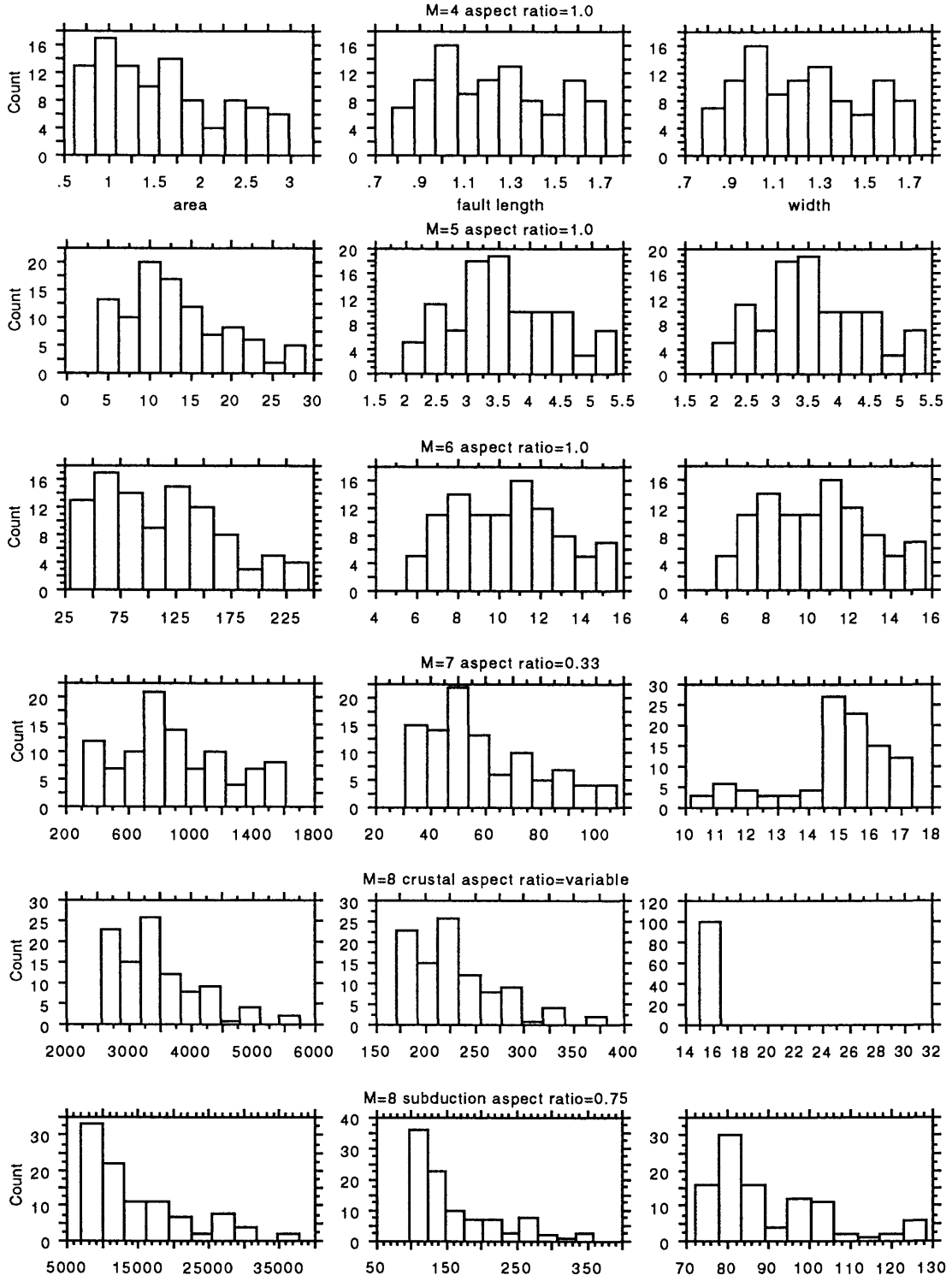

Figure 11 Distributions of fault area (km^2), fault length (km) and width (km) assumed in fitting the data shown for various aspect ratios.

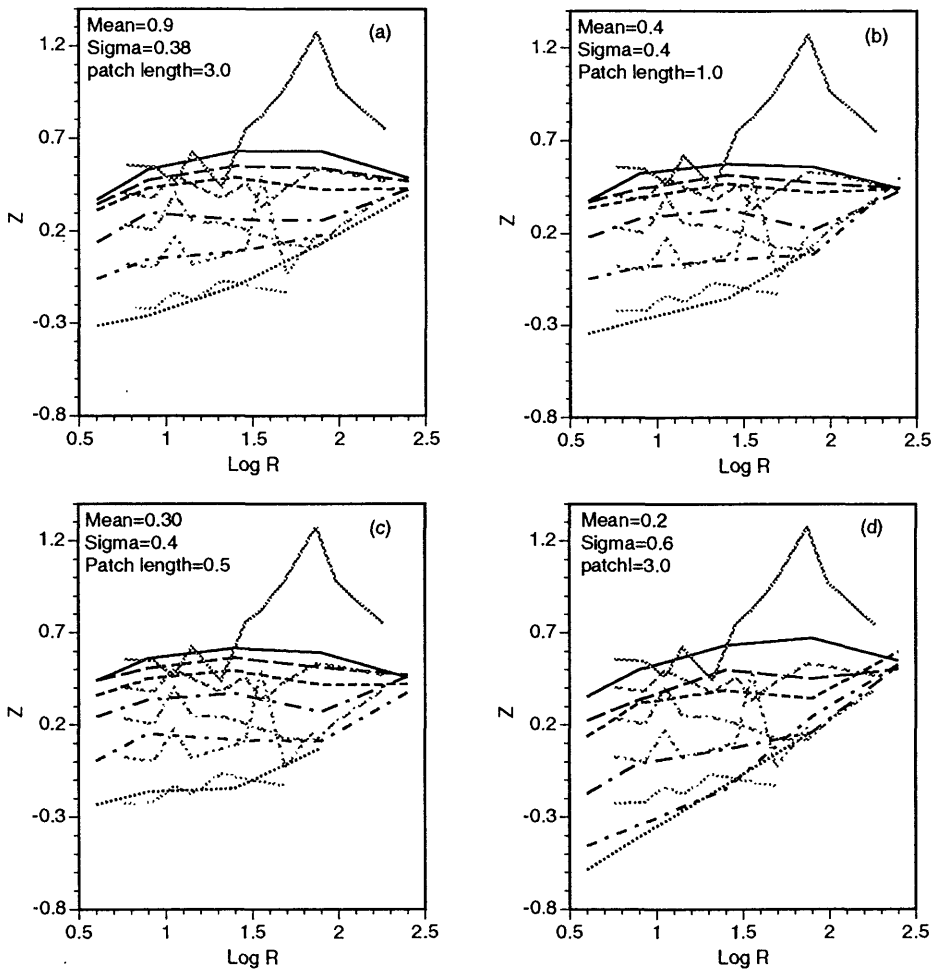

Figure 12 Panels a-d show model fits to the smoothed data for the values of the parameters shown in each panel. These plots show the partial interchangeability of some model parameters, such as patch mean and patch size or mean and sigma. Parameters held constant for all panels are lower limit=0.02; no upper limit; anelastic attenuation, k=0.0013. The grayed lines in each plot are the data, which range in magnitude from M4-8 from bottom to top. The model results are shown as black broken lines ranging from M4-8 crustal and M8 subduction (solid black). No site effects are included in these plots.

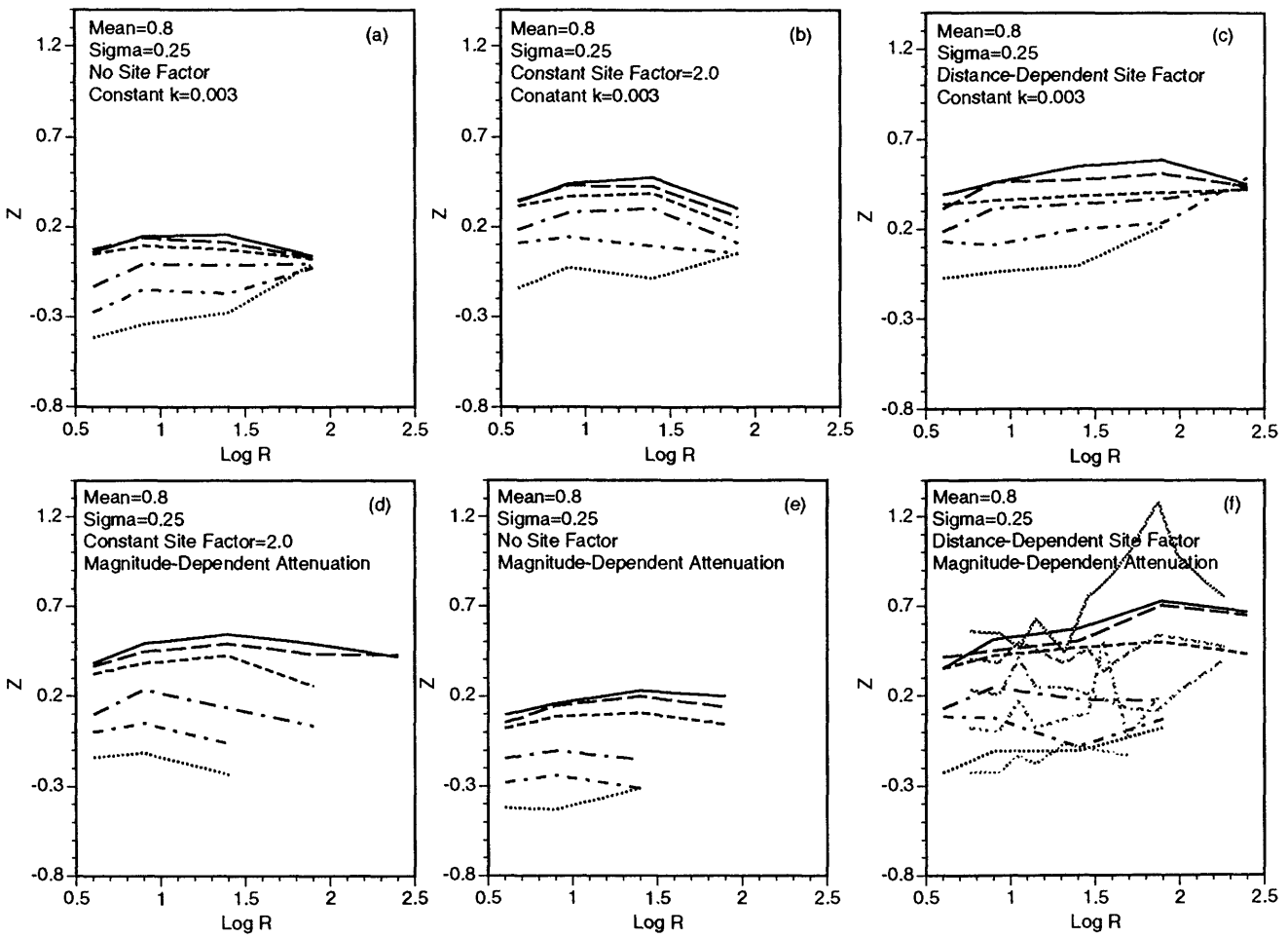

Figure 13 Panels a-c show the effects of various site factors as marked. Panels d-f show the effect on panels a-c of including magnitude-dependent attenuation. The distance-dependent site function is described in the text. The values of k assumed are: M4, 0.012; M5, 0.010; M6, 0.008; M7, 0.0025; and M8, 0.001. Parameters held constant for all panels are lower limit=0.02; no upper limit; patch size=3 km. Panel f shows a comparison of a model result (black lines), including the distance-dependent site factor and magnitude-dependent attenuation, with the smoothed data (grayed lines).

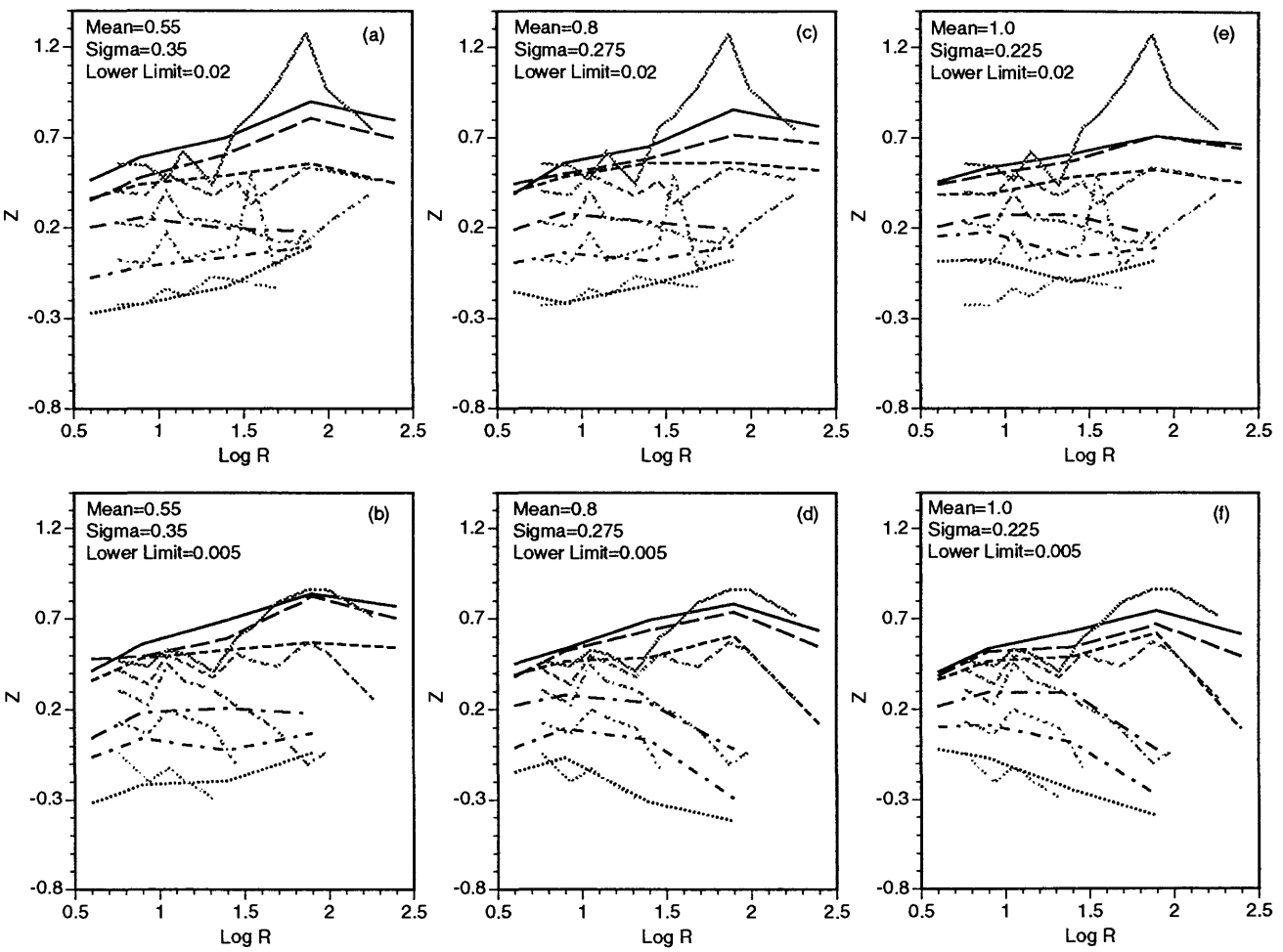

Figure 14 Results of fitting the model to both data representations. The panels on the top are the smoothed data, and the panels on the bottom are the paradigm representation. Panels a, b, e, and f are not considered acceptable fits to the data; panels c and d are our best fits to both data sets without fine tuning the model. The model parameters for these cases are lower limit=0.005 g, no upper limit, patch size=3 km, and distance-dependent site factor and magnitude-dependent attenuation. The values of k assumed are 0.012 for M4, 0.010 for M5, 0.008 for M6, 0.0025 for M7, and 0.001 for M8.

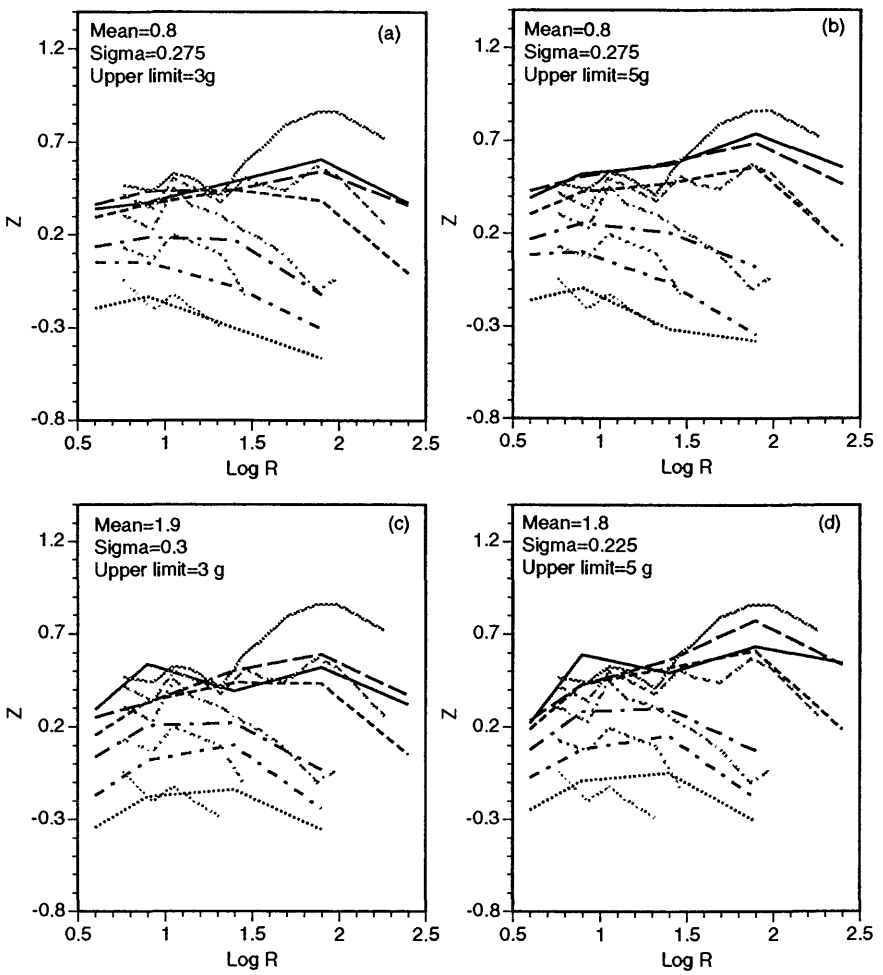

Figure 15 Results of fitting the model to the paradigm data representation including a peak-patch acceleration upper limit (panels a and b) and fitting with both the peak-patch acceleration upper limit and a crustal strength function (panels c and d). These results set the lower limit to 0.005 g, all other parameters are as in figure 14.

Flow Diagram for the Monte Carlo Finite Fault Peak Acceleration Model

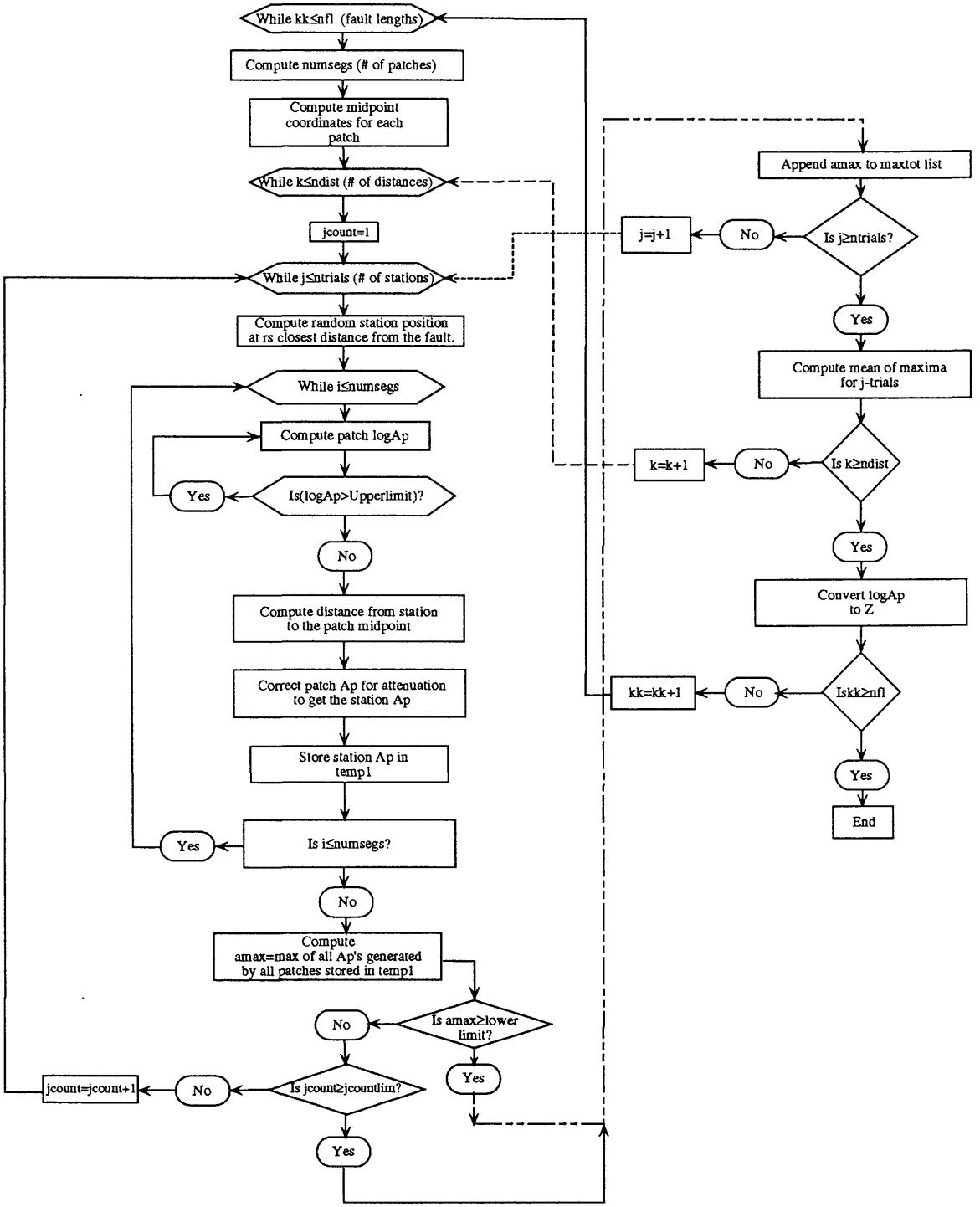

Appendix A